



Nanopositioning Systems for X-ray Optical Instrumentation

Deming Shu

**Advanced Photon Source
Argonne National Laboratory
Argonne, Illinois 60439, U.S.A.**

*With my colleagues at Argonne CNM, APS/XSD, APS/AES, and MSD
for the development of x-ray nanoprobe instruments:*

J. Maser, M. Holt, R. Winarski, C. Preissner, B. Lai, S. Vogt, G. B. Stephenson,

for the development of high precision x-ray monochromators and analyzers:

*T. S. Toellner, E. E. Alp, J. Ilavsky, S. D. Shastri, P. L. Lee, S. Narayanan, and
G. G. Long*

MEDSI/SRI-2008 Workshop for Challenges in Beamline Optics

June 10, 2008

Outline

- **Introduction**
- **Nanometer scale motion control techniques developed at the APS**
 - **Laser Doppler encoder with multiple-reflection optics**
--- Technique for repeatable measurement in sub-nanometer scale
 - **High-stiffness weak-link for linear motion reduction mechanism**
--- Technique for reliable motion in sub-nanometer scale
 - **Real-time closed-loop feedback for active relative vibration control in nanometer scale**
- **Applications for synchrotron radiation instrumentation**
 - **High precision x-ray crystal monochromators and analyzers**
 - **Scanning stage system for hard x-ray nanoprobes**
- **Prepare for more challenges**



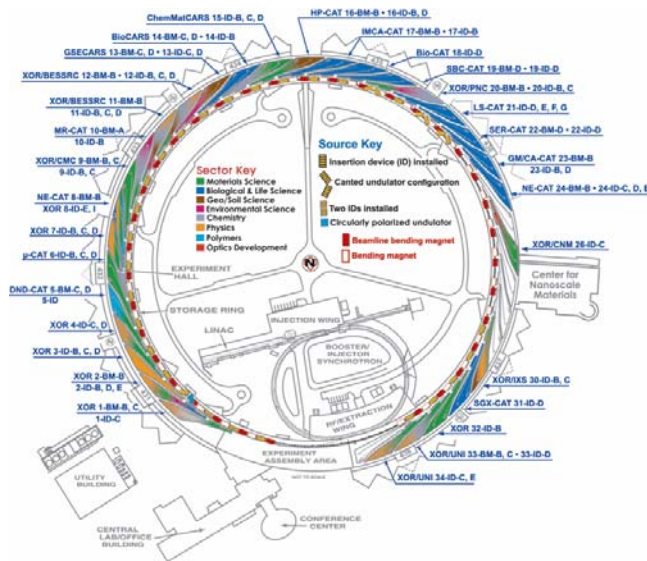
Introduction



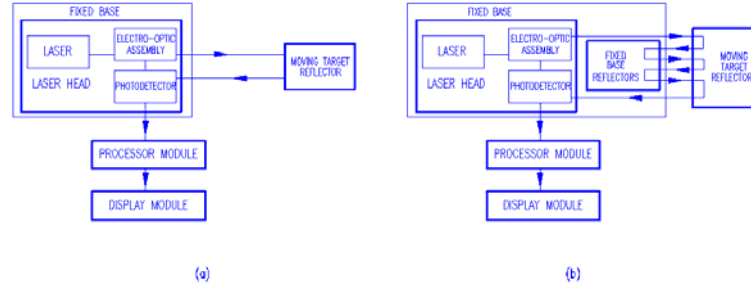
The Advanced Photon Source (APS) at the Argonne National Laboratory is a national user facility for synchrotron radiation research.



Introduction



Laser Doppler encoder with multiple-reflection optics



Since 1998 a prototype laser Doppler linear encoder (LDLE) with multiple reflections has been under development at the APS. With a customized commercial laser Doppler displacement meter (LDDM), this novel linear encoder achieved sub-100-pm sensitivity in a 300-mm measuring range. The LDDM is based on the principles of radar, the Doppler effect, and optical heterodyning. We have chosen a LDDM as our basic system, not only because of its high resolution (2 nm typically) and fast object speed (2 m/s), but also because of its unique performance independent of polarization, which provides the convenience to create a novel multiple-reflection-based optical design to attain sub-100-pm linear resolution.

Laser Doppler encoder with multiple-reflection optics

- A commercial Laser Doppler Displacement Meter (LDDM) system includes four components: a laser head, a processor module, a display module, and a target reflector. The laser head houses a frequency-stabilized HeNe laser, an electro-optic assembly and a photodetector, which functions as a receiver. The laser light reflected by the target is frequency shifted by the motion of the target. The photodetector measures the phase variation caused by the frequency shift, which corresponds to the displacement of the target.

- When the displacement is larger than the half-wavelength, $\lambda/2$, a counter records the total phase changes as:

$$\Delta\phi_{\text{total}} = 2\pi N + \phi, \quad (1)$$

where N is the number of half-wavelengths, and ϕ is the phase angle less than 2π .

Laser Doppler encoder with multiple-reflection optics

The total target displacement, Δz , can be expressed as:

$$\Delta z = \frac{c}{2f_0} (N + \phi/2\pi), \quad (2)$$

where f_0 is the frequency of the laser, and c is the speed of the light.

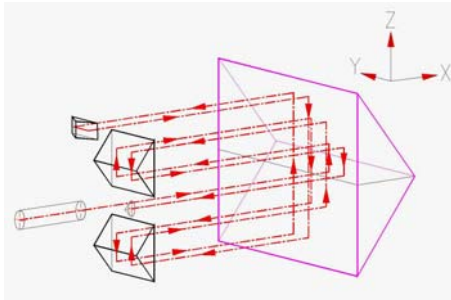
If we make the laser light reflecting back and forth M times between the fixed base and the target before it finally reaches the photodetector, then introducing equation (2) gives

$$\Delta z = \frac{c}{2f_0 M} (N + \phi/2\pi), \quad (3)$$

which indicates that the multiple-reflection optics provides M -times resolution extension power for the system.



Laser Doppler encoder with multiple-reflection optics

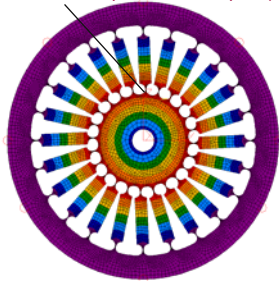


In the self-aligning multiple-reflection optical design for the LDDM system, the heterodyning detector is housed coaxially inside the frequency-stabilized laser source. Instead of a typical single reflection on the moving target, the laser beam is reflected back and forth twelve times between the fixed base and the moving target. The laser beam, which is reflected back to the heterodyning detector, is frequency-shifted by the movement of the moving target relative to the fixed base. With same LDDM laser source and detector electronics, this optical path provides twelve times greater resolution for the linear displacement measurement and encoding. A 0.03 nm resolution was reached by the prototype LDDM system recently.

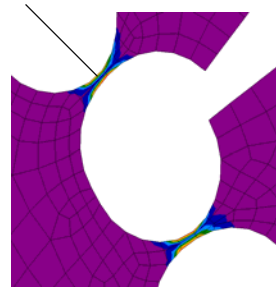
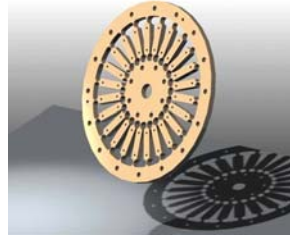


Weak-link mechanism for high-energy-resolution x-ray monochromator

maximum displacement 94 μm (0.25 degree angular motion)



maximum von Mises stress 175 MPa



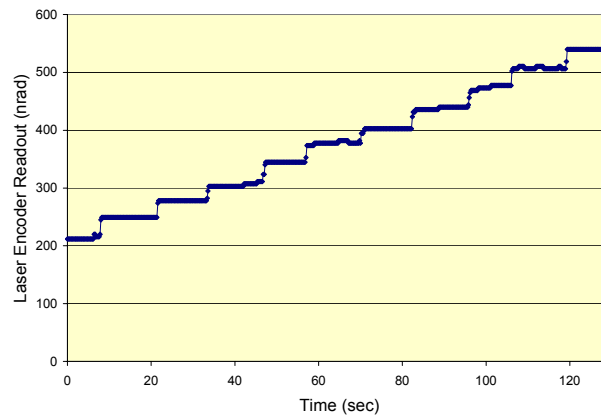
Unlike traditional kinematic linear spring mechanisms, the overconstrained weak-link mechanism provides much higher structural stiffness and stability. Using a laminar structure configured and manufactured by chemical etching and lithography techniques, we are able to design and build a planar-shape, high-stiffness, high-precision weak-link mechanism.

The precision of modern photochemical machining processes using lithography techniques makes it possible to construct a strain-free (or strain-limited) overconstrained mechanism on thin metal sheets. By stacking these thin-metal weak-link sheets with alignment pins, we can construct a solid complex weak-link structure for a reasonable cost.



High-stiffness weak-link mechanism

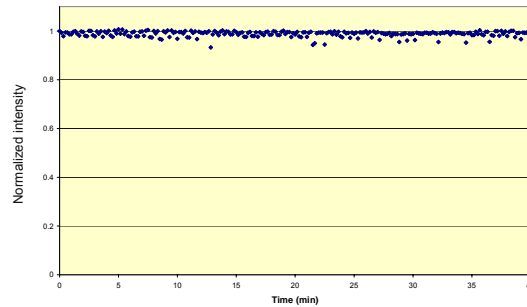
- Sensitivity test with a laser Doppler encoder
A test with 33 nrad average step size



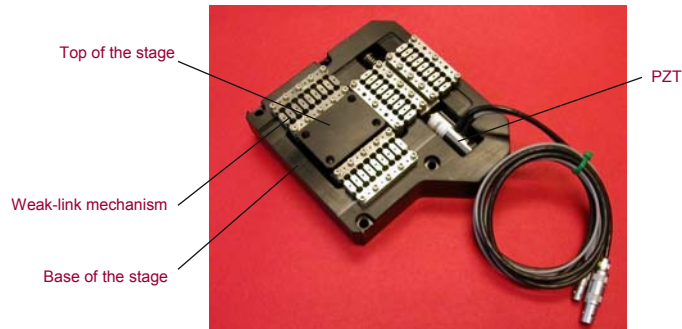
High-stiffness weak-link mechanism

- Stability result from a x-ray experiment

Relative intensity measured by an ionization chamber after the high-resolution monochromator (1-meV bandwidth) as a function of time. The data are corrected for the decaying current in the storage ring.



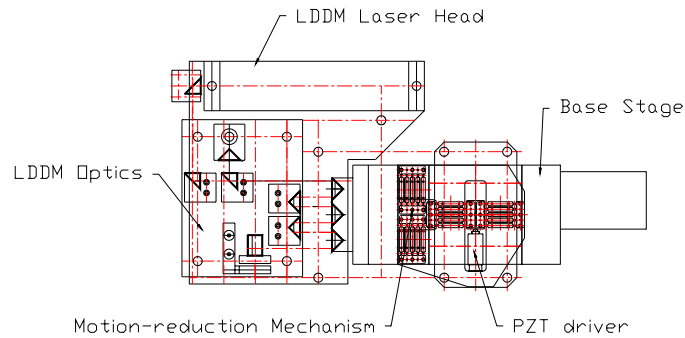
High-stiffness weak-link mechanism for linear motion reduction



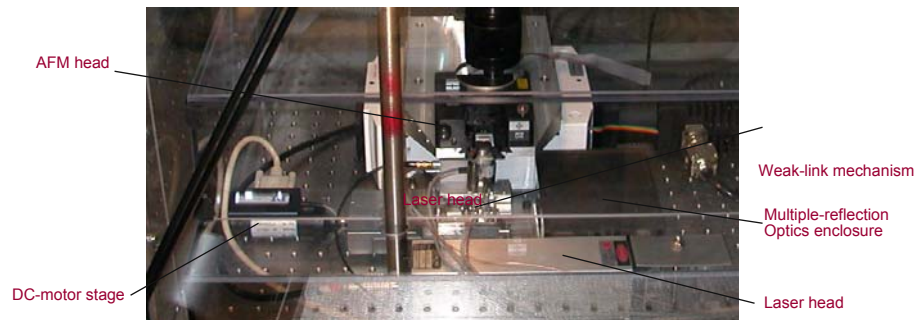
Using the same technique described in the section for the weak-link mechanism for a high-energy-resolution monochromator, we have developed a novel stage using a high-stiffness weak-link mechanism to perform linear motion closed-loop control at the sub-100-pm level with micron-level travel range. The structure consists of four groups of overconstrained weak-link parallelogram mechanisms made with lithography techniques. Driving sensitivity better than 30 pm was demonstrated with this weak-link linear-motion-reduction mechanism with a 1-micron travel range.

A one-dimensional linear actuator system with subnanometer closed-loop control resolution and centimeters travel range for an atomic force microscope

Prototype of a laser Doppler linear actuator system (LDLA) with sub-angstrom sensor resolution and positioning resolution over a 50-mm travel range.



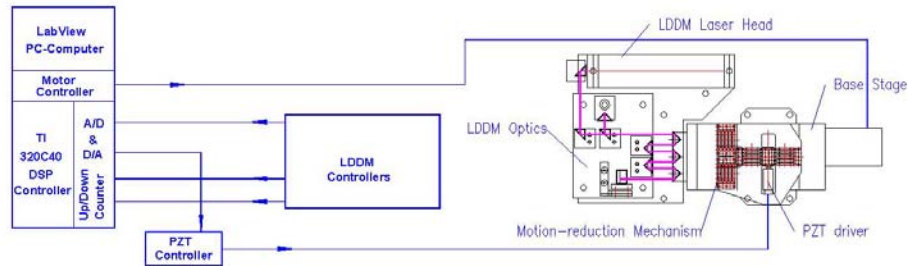
A one-dimensional linear actuator system with subnanometer closed-loop control resolution and centimeters travel range for an atomic force microscope



A one-dimensional linear actuator system based on the above high-stiffness weak-link technique and LDDM with multiple-reflection optics has been tested. This photo shows the one-dimensional laser Doppler linear actuator (LDLA) system for an atomic force microscope. In this coarse/fine closed-loop control setup, a PZT-driven motion-reduction mechanism was mounted on the top of a DC-motor-driven stage to drive the motion object (in this example, a sample holder for an atomic force microscope).



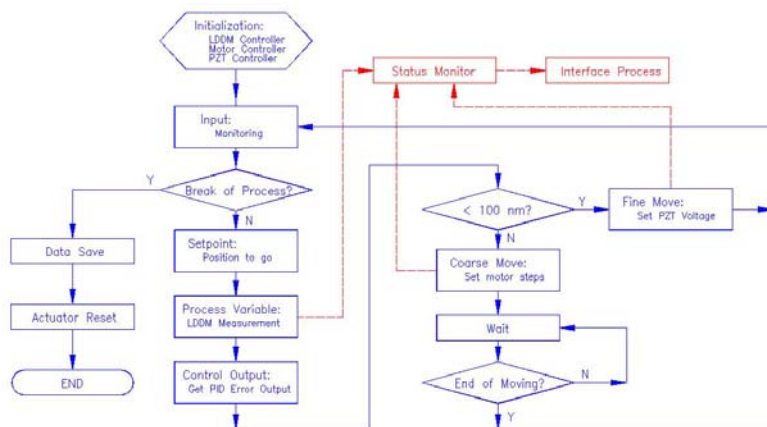
A one-dimensional linear actuator system with subnanometer closed-loop control resolution and centimeters travel range for an atomic force microscope



A laser Doppler displacement meter with an optical resolution extension assembly was used to measure the sample holder motion in the 25-mm range with sub-100- μm resolution. The LDDM position signal is fed back through a TI 320C40 DSP controller to control the PZT. The PZT drove the motion-reduction mechanism with sub-100- μm resolution to stabilize the motion. The DSP controller also provides digital filtering for the LDDM position signal. The system control computer synchronized the stage position and PZT feedback lock-in point with the LDDM position signal.



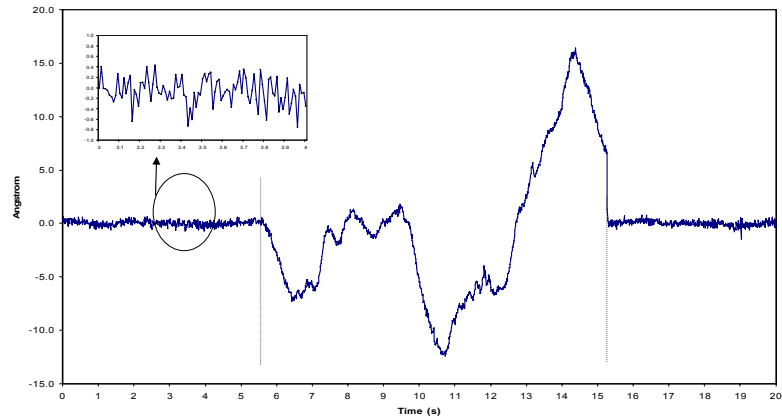
A one-dimensional linear actuator system with subnanometer closed-loop control resolution and centimeters travel range for an atomic force microscope



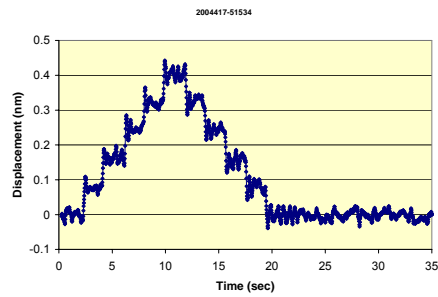
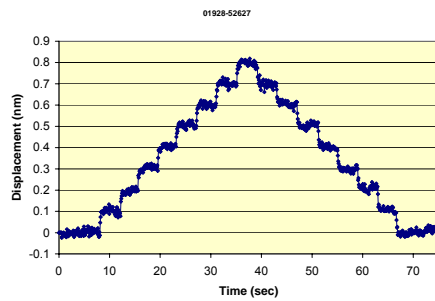
A one-dimensional linear actuator system with subnanometer closed-loop control resolution and centimeters travel range for an atomic force microscope

Test of a LDLA closed-loop feedback system

Comparison of Open loop and Closed loop



A one-dimensional linear actuator system with subnanometer closed-loop control resolution and centimeters travel range for an atomic force microscope

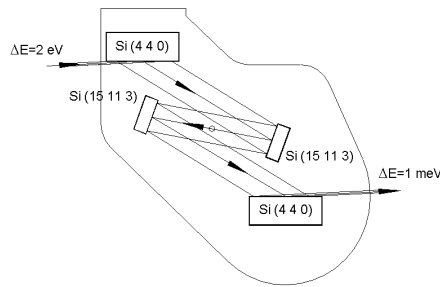


Resolution test of the one-dimensional laser Doppler linear actuator closed-loop control system. A series of 100-pm (left side) and 80-pm (right side) steps have been demonstrated.



Artificial Channel-Cut Crystal Mechanism

In 1999, to overcome the obstacles in developing a 4-crystal in-line high-resolution hard x-ray monochromator using a nested channel-cut crystal geometry with meV bandpass, the first high-stiffness weak-link mechanism with stacked thin-metal sheets was developed for the APS high-energy-resolution beamline 3-ID. The precision and stability of this mechanism allowed us to align or adjust an assembly of crystals to achieve the same performance as a single channel-cut crystal, so we called it an “artificial channel-cut crystal.”



Weak-link mechanism for high-energy x-ray monochromator at APS 1-ID-B



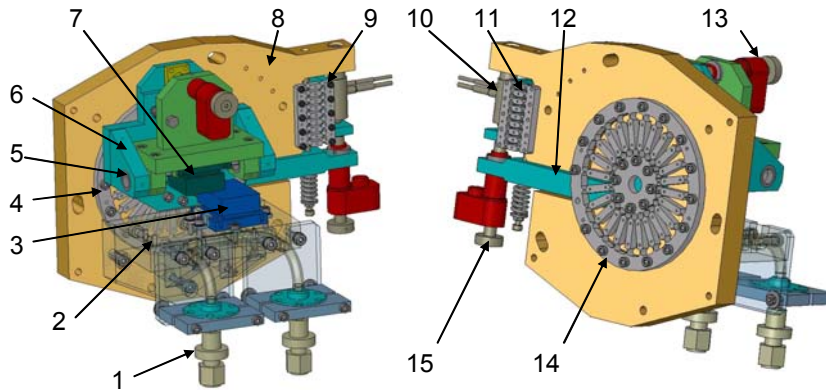
Photograph of a high-energy x-ray monochromator with four crystal reflections constructed at APS XOR beamline 1-ID-B. It shows a high-energy (50-100 keV) high-resolution x-ray monochromator with four crystal reflections constructed at APS beamline 1-ID-B, which has been used for resonant powder diffraction* and stress/strain studies**.

* Y. Zhang, A. P. Wilkinson, P. L. Lee, S. D. Shastri, D. Shu, D. -Y. Chung, M. G. Kanatzidis, J. Appl. Cryst. 38, 433-441 (2005).

** B. Jakobsen, H. F. Poulsen, U. Lienert, J. Almer, S. D. Shastri, H. Sorensen, C. Gundlach, W. Pantleon, Science 312, 889-892 (2006).



UHV-Compatible Artificial Channel-Cut Crystal Mechanism



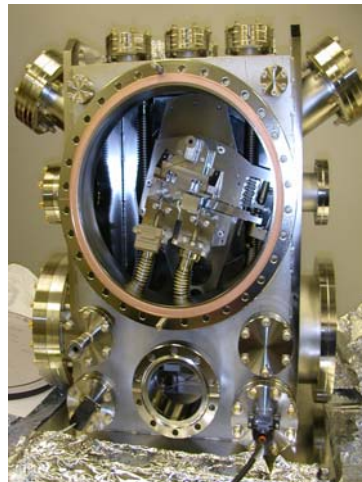
Front side and back side views of a 3-D model for a typical high-stiffness weak-link mechanism for an “artificial channel-cut crystal”. (1) Cooling tube; (2) First crystal holder; (3) First crystal; (4) and (14) Rotary weak-link modules; (5) flexure bearing; (6) Second crystal holder; (7) Second crystal; (8) Base plate; (9) and (11) linear weak-link modules; (10) PZT actuator; (12) Sine bar; (13) and (15) Picomotor™ actuators. [9]



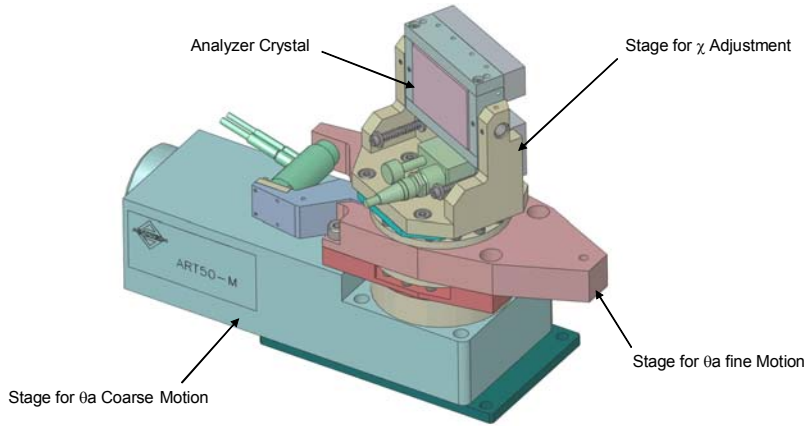
UHV-Compatible Artificial Channel-Cut Crystal Mechanism

TABLE 2. Mechanical design specifications of the double-bounce Ge(111) monochromator

| | |
|--|--|
| Main sine bar driver type | Ceramic-motor-driven linear stage with linear grating encoder |
| Main sine bar rotation range | 13 degree |
| Main sine bar length | 233.7 mm |
| Main sine bar rotation resolution | 0.02 arc sec |
| Main sine bar rotation positioning reproducibility | 0.5 arc sec or better |
| ACCM sine bar driver type | Fine: PZT actuator with strain sensor, Coarse: Picomotor™ actuator |
| ACCM sine bar rotation range | Fine: 27 arc sec, Coarse: 0.5 degree |
| ACCM sine bar length | 115 mm |
| ACCM sine bar rotation resolution | 0.005 arc sec (with PZT actuator) |
| ACCM sine bar rotation positioning reproducibility | 0.2 arc sec or better (with PZT actuator) |
| Vacuum compatibility | UHV compatible |



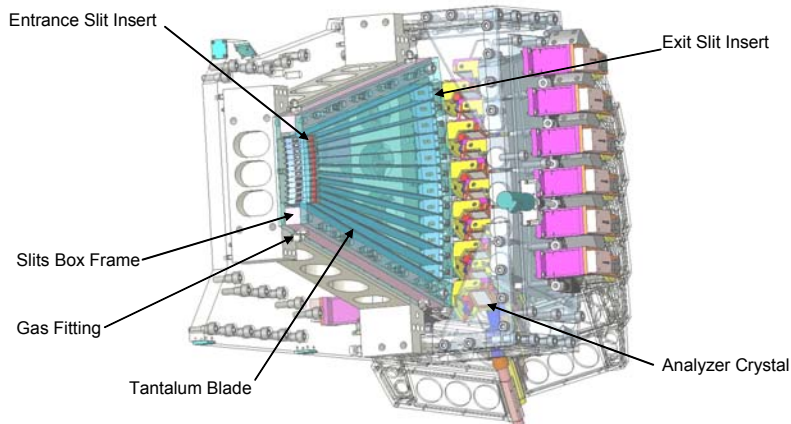
Stages for high-resolution crystal analyzer



For each of the analyzer crystals, there are three positioning devices stacked together to control the crystal's angle θ_a coarse motion, angle θ_a fine motion, and angle χ adjustment. A commercial rotary stage ART-50 from Aerotech™ Inc. U.S.A. is applied for the analyzer crystal's angle θ_a coarse positioning.



X-ray slits array

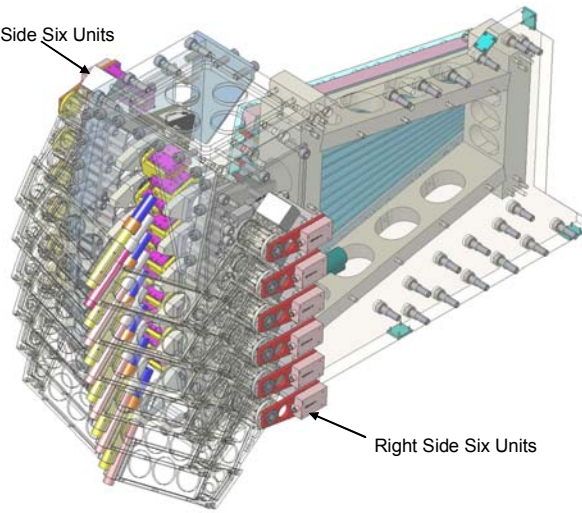


The slits box consists of an aluminum slits box frame, tantalum x-ray insulating blades, and 24 slit inserts. The slit inserts are precisely exchangeable. A set of slit inserts is manufactured to cover the tantalum knife-edge slit size range from 0.2 mm to 3 mm for various applications.



Twelve-analyzer and detector system

Left Side Six Units

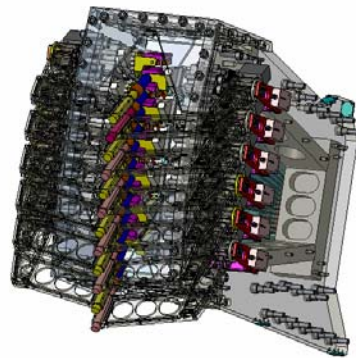


Right Side Six Units

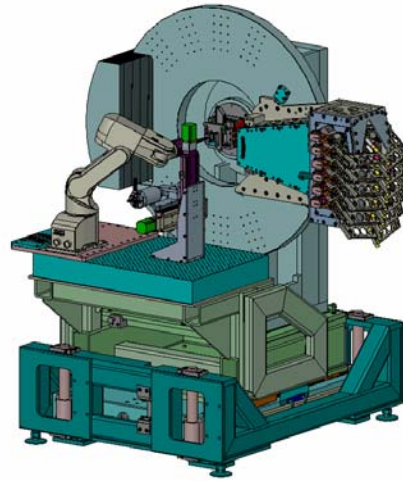


We grouped the twelve analyzers and detectors into two sub-assemblies: left side six units and right side six units.

Twelve-analyzer and detector system

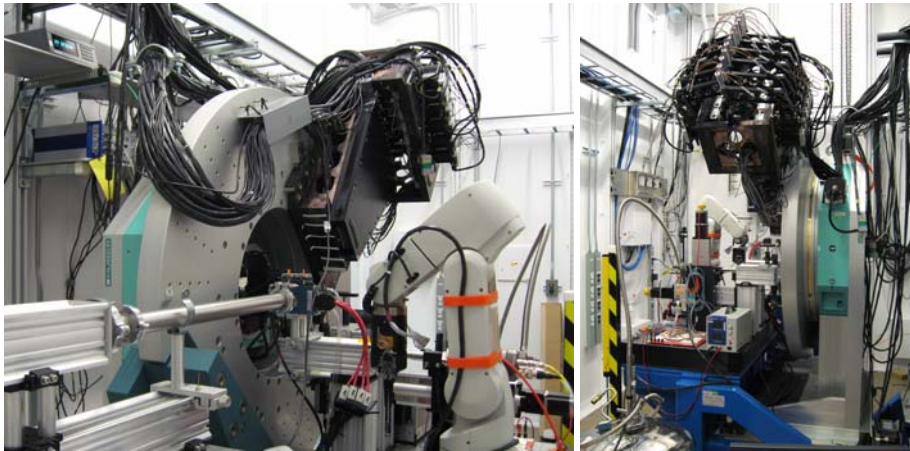


General layout



A 3-D model of the high-resolution diffractometer with 12-analyzer/detector system

General layout



The high-resolution diffractometer has a dimension of 2600 mm (H) X 2100 mm (L) X 1700 mm (W). The main circle of the goniometer has a vertical mounting disk with an outside diameter of 1200 mm.

Introduction for ANL CNM nanoprobe project at APS

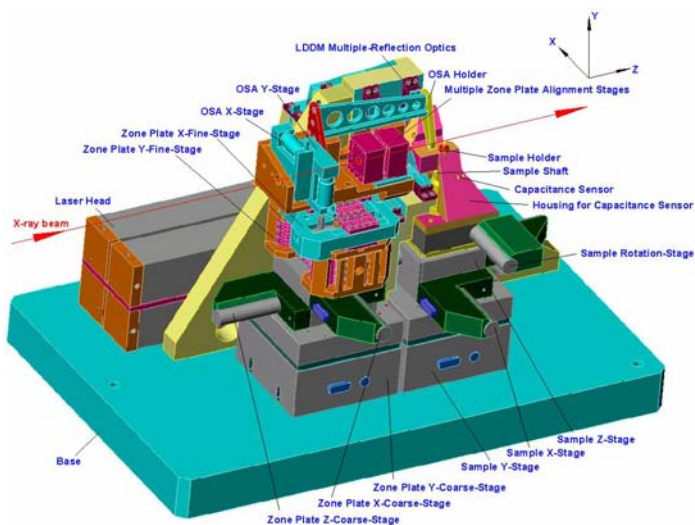
Centerpiece of the X-ray Characterization Facilities at the CNM

- The goal of Argonne's Center for Nanoscale Materials (CNM) is to create, characterize, and understand the behavior of new functional materials on the nanoscale.
- The beamline is one of the premiere tools available to researchers at the CNM

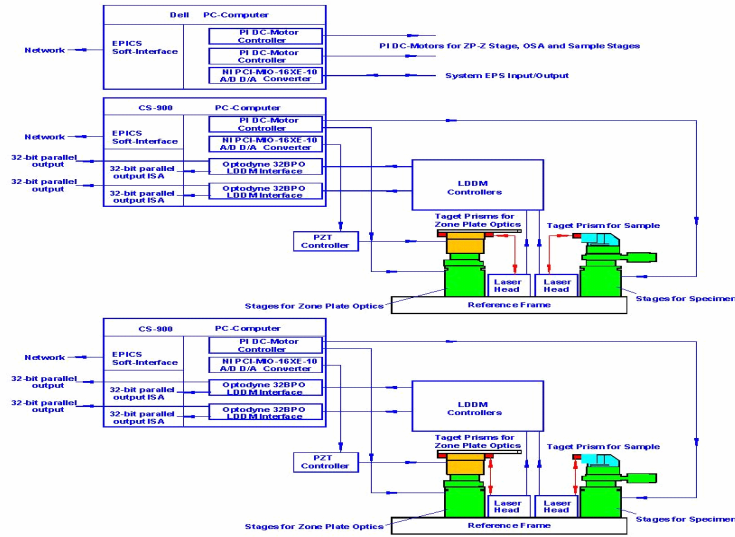


- Located adjacent to the CNM building at Sector 26 of the Advanced Photon Source (APS)
- Developed in partnership with the APS to build a state-of-the-art beamline that will provide stable, powerful, and coherent x-ray illumination for research at the nanoscale

Design of an X-ray Nanoprobe Prototype



Design of an X-ray Nanoprobe Prototype



Design of an x-ray nanoprobe prototype



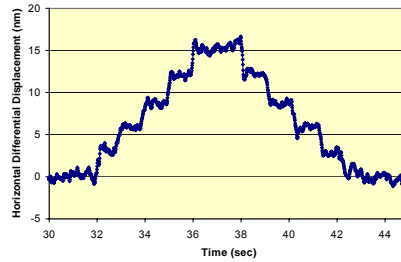
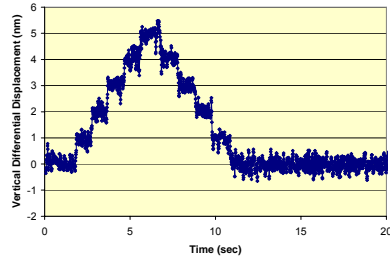
We started the x-ray nanoprobe prototype online commissioning in August 2003. These are photographs of the prototype at the APS 8-ID-E experimental station (left) and in a test laboratory (right).



Design of an x-ray nanoprobe prototype

TABLE 1. Design specifications for the x-ray nanoprobe prototype laser Doppler encoder system

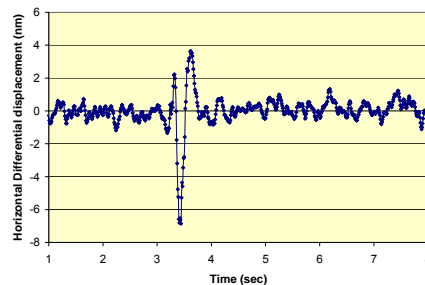
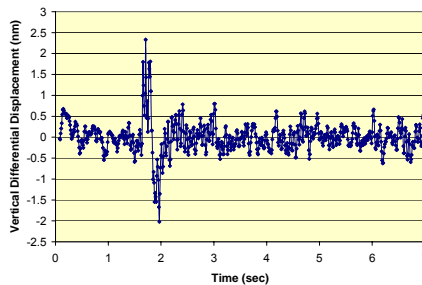
| | |
|---------------------------------|---|
| Overall Dimension (mm) | 450 (X) x 450 (Y) x 650 (Z) |
| Encoder type | Two-dimensional differential laser Doppler encoder with multiple- reflection Optics [4,5,6,7] |
| Laser source | Frequency stabilized He-Ne Class II |
| Multiple-reflection optics path | 1.6 |
| Displacement resolution (nm) | 0.125 |
| Measurement range (mm) | 12 (X) x 12 (Y) x 12 (Z) |



Closed-loop differential displacement test for the prototype scanning stage system for the x-ray nanoprobe at the APS 8-ID-E station, horizontal: left side; vertical: right side. A series of 1-nm and 3-nm differential vertical and horizontal displacement steps (between zone-plate holder and sample holder) have been demonstrated with closed-loop control.



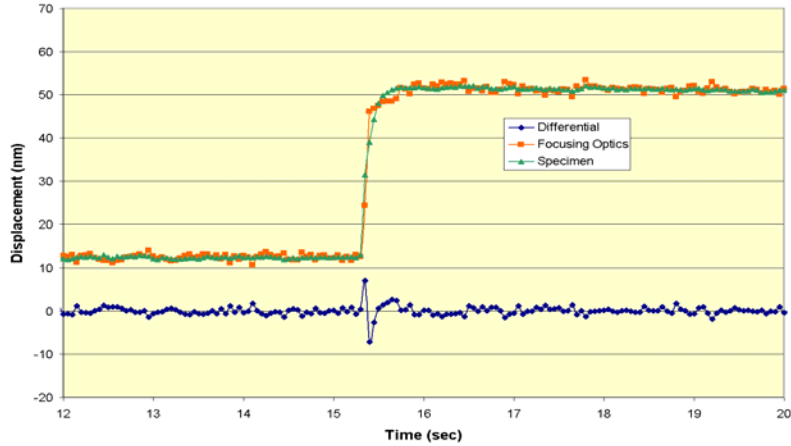
Design of an x-ray nanoprobe prototype



Active vibration control test for the prototype scanning stage system for the x-ray nanoprobe at the APS 8-ID-E station, vertical: left side; horizontal: right side. During this test, the closed-loop control system performed a damping action to a single external mechanical disturbance (an 80-kg mass dropped to the floor from a 0.2-m height at a distance of 3 m).

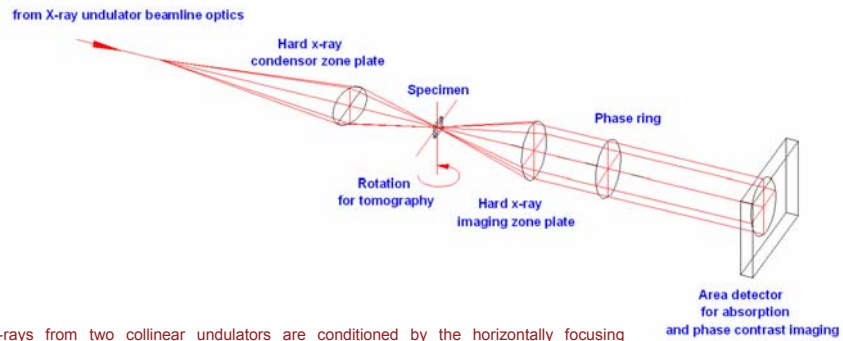


Design of an x-ray nanoprobe prototype



Operating modes of the Argonne nanoprobe instrument

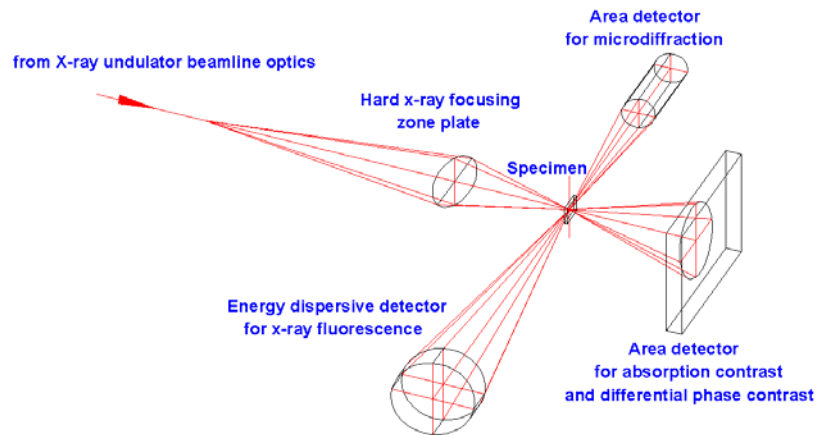
Full-Field Transmission Mode



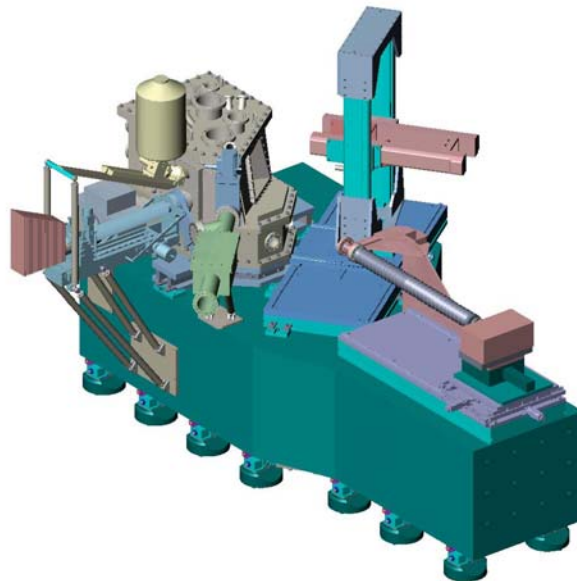
X-rays from two collinear undulators are conditioned by the horizontally focusing nanoprobe mirror system, followed by a beam defining aperture and a crystal monochromator. Switch between scanning probe mode and full-field transmission mode is accomplished by change of the size of the beam defining aperture, and change of configuration of the zone plates in the nanoprobe instrument.

Operating modes of the Argonne nanoprobe instrument

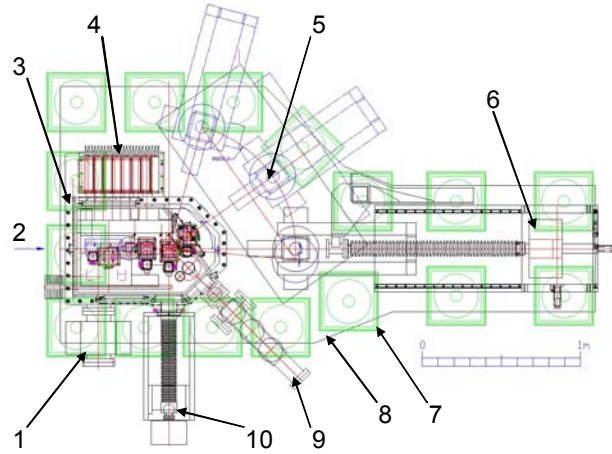
Scanning nanoprobe Mode



Introduction for ANL CNM nanoprobe project at APS



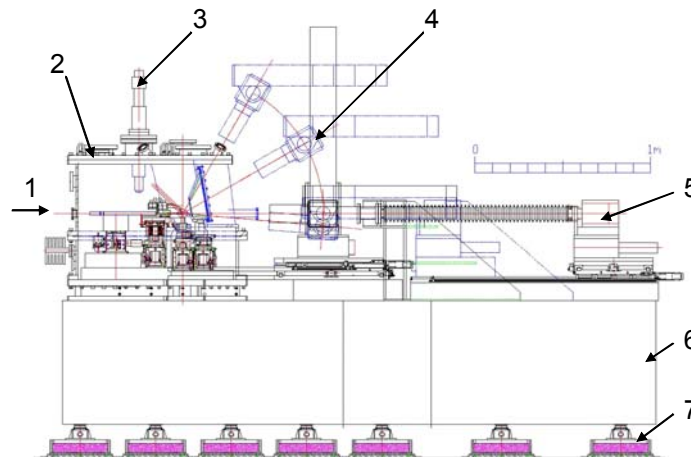
Mechanical general layout design for CNM nanoprobe instrument



Top view of the hard x-ray nanoprobe instrument. (1) Ion pump; (2) Incident beam; (3) Instrument Chamber; (4) Laser head for LDDM; (5) Diffraction detector; (6) Transmission imaging detector; (7) Isolators below base; (8) Granite base; (9) Airlock for specimen exchange; (10) Fluorescence detector.



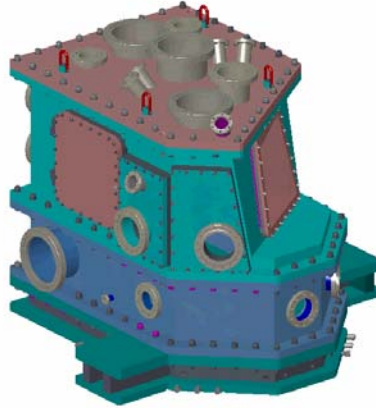
Mechanical general layout design for CNM nanoprobe instrument



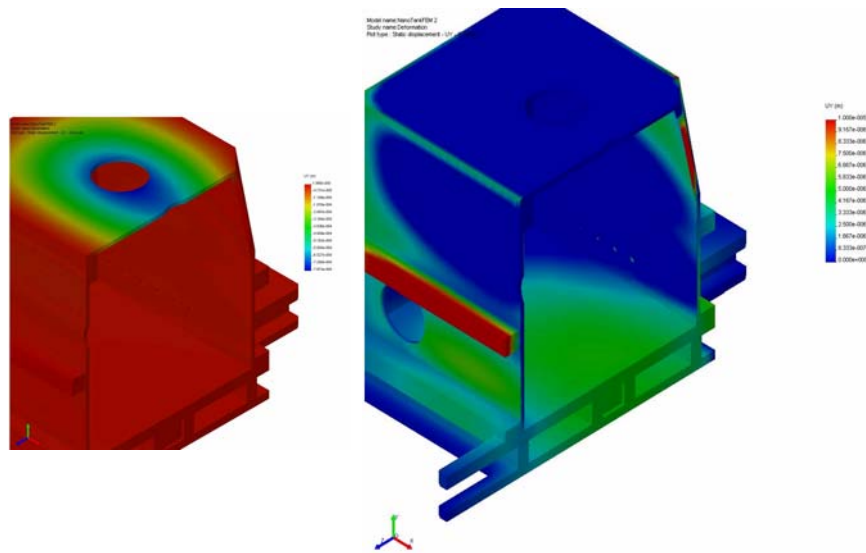
Side view of the hard x-ray nanoprobe instrument. (1) Incident beam; (2) Instrument chamber; (3) Optical microscope; (4) Diffraction detector; (5) Transmission imaging detector; (6) Granite base; (7) Isolators.



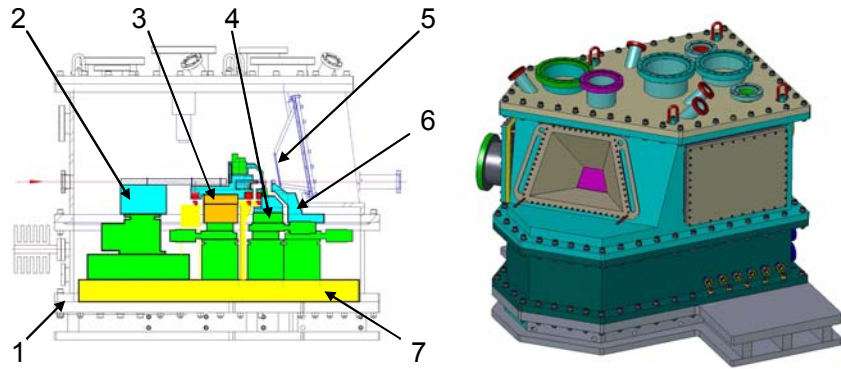
Positioning stage and encoder systems in central instrument chamber



Instrument chamber and invar reference base



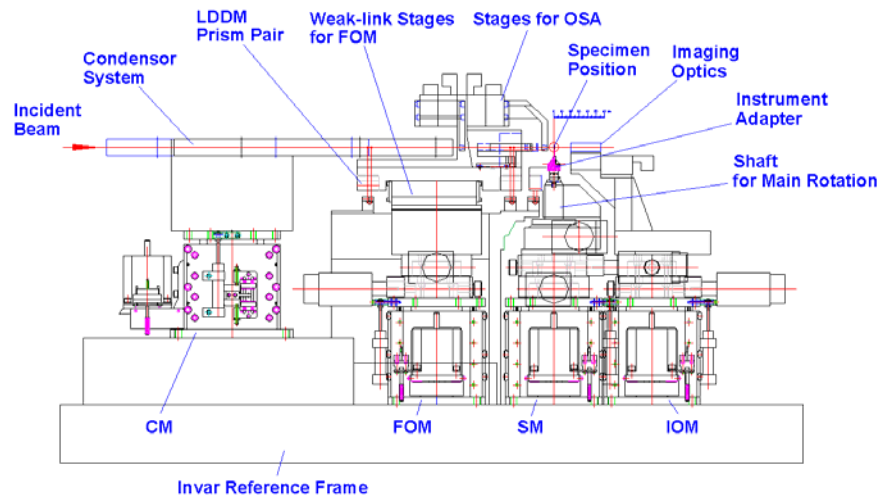
Positioning stage and encoder systems in central instrument chamber



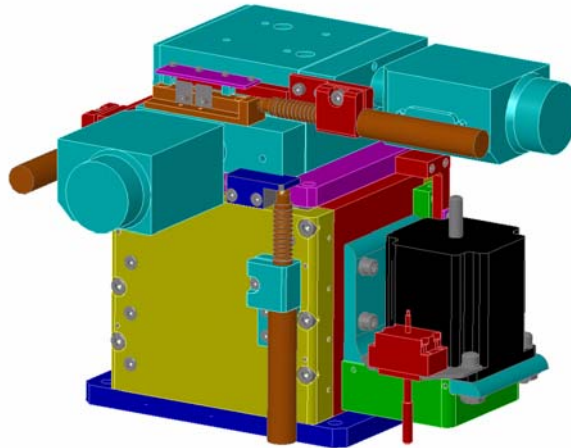
Left: A schematic side view of the nanoprobe instrument chamber. (1) Vacuum chamber; (2) CM; (3) FOM; (4) SM; (5) Beryllium window; (6) IOM; (7) Invar reference base. Right: A 3-D model of the nanoprobe instrument chamber.



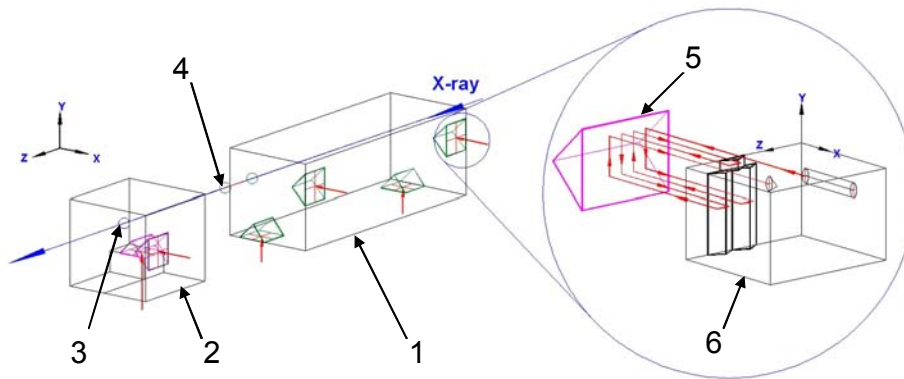
Positioning stage and encoder systems in central instrument chamber



Scanning stages for focusing optics module

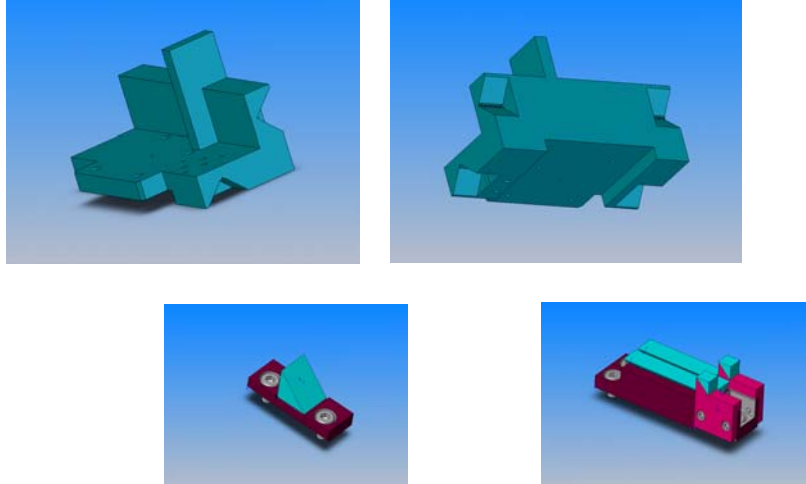


Laser Doppler encoders for differential 2D positioning and active vibration control

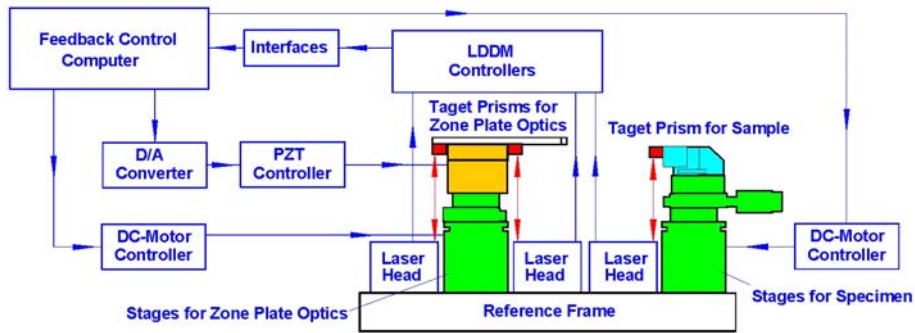


Schematic of the six-LDDM encoder system for the two-dimensional differential position encoding between the FOM and SM. (1) Prism holder for zone-plate optics; (2) Prism holder for sample stage; (3) Sample location; (4) Zone-plate optics locations; (5) Prism on the stage; (6) Prism group on the reference frame.

Laser Doppler encoders for differential 2D positioning and active vibration control



Laser Doppler encoders for differential 2D positioning and active vibration control



Schematic of differential positioning feedback control in the vertical (Y) direction. For the differential feedback positioning control in the vertical (Y) direction, two LDDMs are applied to the FOM and SM in the Y direction. Since the reference frame defines the coordinate system of the nanoprobe, all positions are measured with respect to this frame. To perform a differential measurement between the stage groups for FOM and SM in the Y direction, a DSP-based feedback control computer is used as a control console to collect the position information from the three LDDMs with a positioning update rate of 937 kHz. The DSP computes the position differences between the two stage groups and determines the discrepancy between the actual and desired differential position between the zone-plate optics and sample, and feeds back differential position-correction signals through a proportional-integral-derivative (PID) loop to the PZT-driven weak-link stage on the FOM. Differential scanning motion can be activated by controlling the desired differential position value. In the case of large-range scanning activity, a relay mechanism is implemented into the control software to ensure a smooth transition between the PZT-driven weak-link fine stage and the DC-motor-driven coarse translation stage.

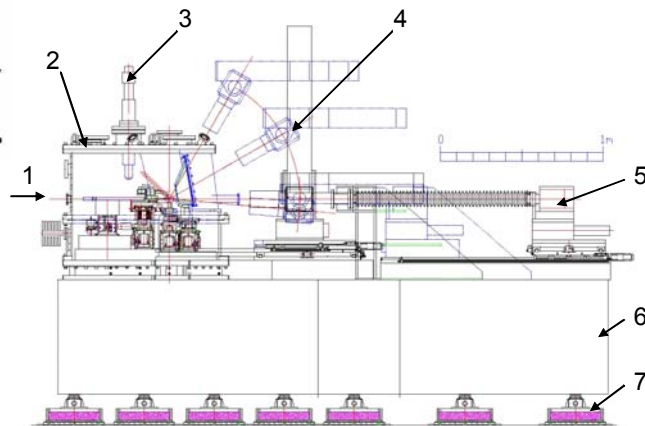
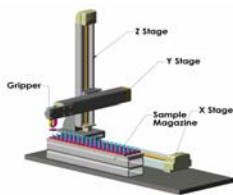


Design challenges for the microdiffraction with nanoprobe

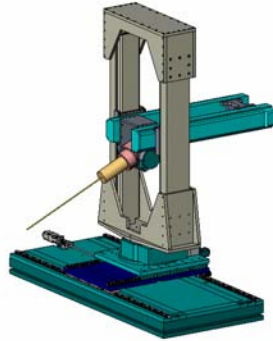
Limited by the geometric configuration of the nanoprobe instrument, it is not feasible to use a traditional goniometer to achieve the motions needed for a microdiffraction detector.



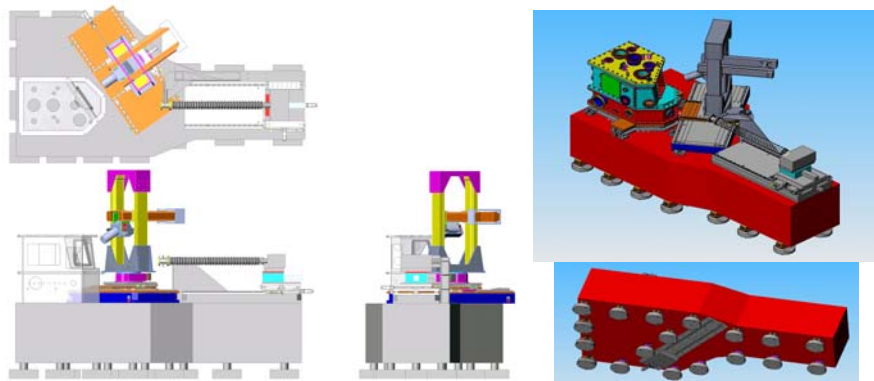
Supporting stages for fluorescence, transmission and diffraction detector systems



Detector manipulator with 12-kg load capacity



Mass center dynamic balance for the detector manipulator



To optimize the nanoprobe instrument positioning stability, several heavy metal balance blocks are applied on the nanoprobe supporting system. They are mounted on motorized stages under the granite table. Synchronized with the detector manipulator motion, the balancing blocks keep the nanoprobe mass center position stable.

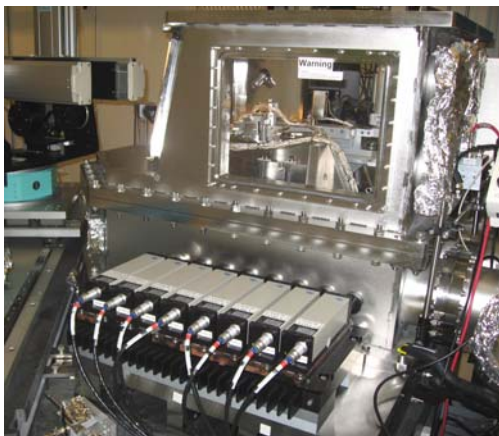
Commissioning of the Argonne nanoprobe instrument



Courtesy of: 



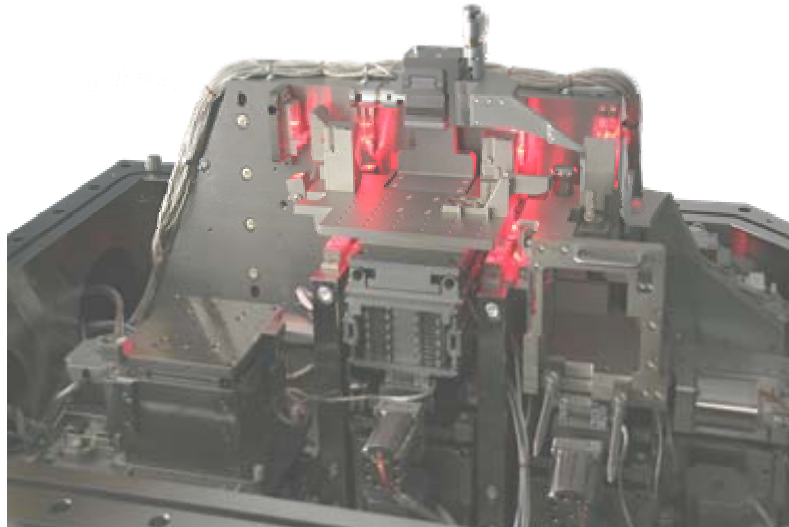
Commissioning of the Argonne nanoprobe instrument



Courtesy of: 



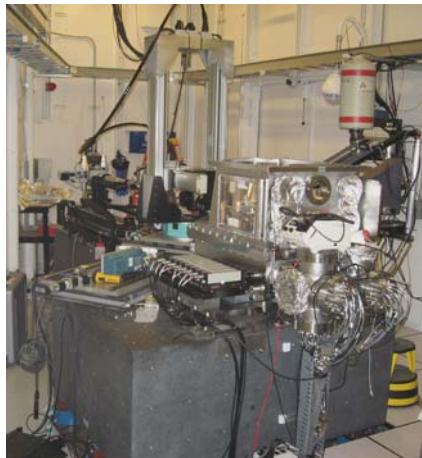
Commissioning of the Argonne nanoprobe instrument



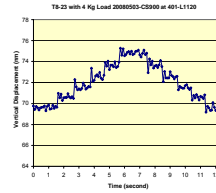
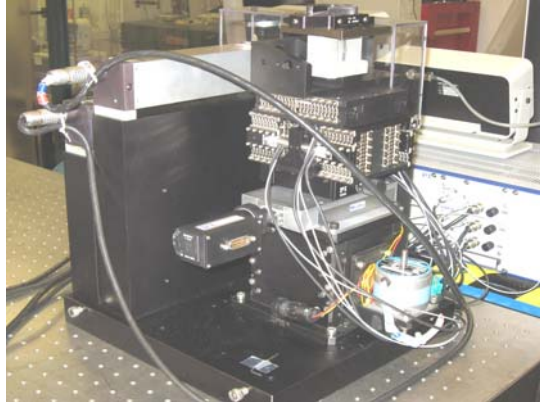
Courtesy of:  xradia



Commissioning of the Argonne nanoprobe instrument



Commissioning of the Argonne nanoprobe instrument



A nanopositioning diagnostic setup has been built to support the CNM nanoprobe instrument commissioning process at the APS. Its laser Doppler interferometer system provides subnanometer positioning diagnostic resolution with large dynamic range. A set of original APS designed ultraprecision PZT-driven weak-link stages with high stiffness motor-driven stages has been tested with this diagnostic setup.



Preparing for more challenges

Example:

The Recent developments in hard x-ray focusing on the nanometer scale with linear multilayer Laue lenses (MLLs) as reported by H. C. Kang et al. have demonstrated a promising new x-ray optic for focusing hard x-rays in a few nanometers. Using tilted partial MLL structures, a one-dimensional focus as small as 16 nm with efficiencies up to 44% has been performed with 19.5-keV synchrotron radiation [26,27]. The high efficiencies should make it practical to produce a point focus using two MLLs in a crossed configuration [28]. A precision multidimensional alignment apparatus is needed for this challenging technical approach.

Deming Shu, Hanfei Yan, and Jorg Maser, Mechanical design of a multi-dimensional alignment system for an MLL system with nanometer-scale 2-D focusing, to be published in Nucl. Instrum. And Meth. for proceedings of SRI-2008.



Acknowledgments

Helps from Argonne National Laboratory:

M. Muscia, A. Nyman, D. Nocher, R. Ranay.

Many thanks to: W. Yun and staff members at XRADIA, Inc.

***C. Jacobsen (NSLS),
Y. Dabin (ESRF), J. Susini (ESRF),
T. Warwick (ALS), T. Tyliszczak (ALS), J. Kirz (ALS),***

This work was supported by the U.S. Department of Energy, Office of Science, Office of Basic Energy Sciences, under Contract No. DE-AC02-06CH11357.



References

- [1] T. S. Toellner, T. Mooney, S. Shastri, and E. E. Alp, SPIE Proc. vol. 1740 (1992) pp. 218.
- [2] E. E. Alp et al., Hyperfine Interactions 90 (1994) pp. 323.
- [3] D. Shu, Y. Han, T. S. Toellner, and E. E. Alp, Proc. SPIE, Vol. 4771 (2002) 78-90
- [4] D. Shu, E. E. Alp, J. Barraza, and T. M. Kuzay, Proc. SPIE, Vol.3429 (1998) 284-292
- [5] U.S. Patent granted No. 6,607,840, D. Shu, T. S. Toellner, and E. E. Alp, 2003
- [6] LDDM is a trademark of the Optodyne Inc., 1180 Mahalo Place, Compton, CA 90220, U.S.A.
- [7] D. Shu, T. S. Toellner, and E. E. Alp, Nucl. Instrum. and Methods A 467-468, 771-774 (2001)
- [8] Instruction manual, Physik Instrumente GmbH & Co., Germany, 2003
- [9] Picomotor is a trademark of Newfocus Co., California
- [10] D. Shu et al., MEDSI 2002, APS, Chicago, U.S.A., 2002
- [11] D. Shu, MEDSI 2004, ESRF, Grenoble, France, 2004
- [12] T. S. Toellner, APS Science 2004, ANL-05/04, p. 130
- [13] S. Narayanan et al., SRI-2006 Conf. Proc. 879, AIP (2007) 911-914.
- [14] Y. Zhang, A. P. Wilkinson, P. L. Lee, S. D. Shastri, D. Shu, D. -Y. Chung, M. G. Kanatzidis, J. Appl. Cryst. 38, 433-441 (2005).
- [15] B. Jakobsen, H. F. Poulsen, U. Lienert, J. Almer, S. D. Shastri, H. Sorensen, C. Gundlach, W. Pantleon, Science 312, 889-892 (2006).
- [16] J. Ilavsky et al., SRI-2006 Conf. Proc. 879, AIP (2007) 1833-1836.
- [17] P. Lee, M. A. Beno, D. Shu, M. Ramanathan, J. F. Mitchell, J. D. Jorgensen, and R. B. Von Dreele, SRI 2003 Conf. Proc. 705, AIP (2004) 388-391.
- [18] U.S. Patent granted No. 5,896,200, D. Shu, 1999
- [19] U.S. Patent granted No. 6,822,733, D. Shu, 2004.
- [20] D. Shu et al., SRI-2006 Conf. Proc. 879, AIP (2007) 1073-1076.
- [21] D. Shu et al., SRI-2006 Conf. Proc. 879, AIP (2007) 1321-1324.
- [22] Catalog and exhibition, Xradia, Inc., Concord, CA 94520, 2008
- [23] U.S. Patent granted No. 6,984,335, D. Shu, T. S. Toellner, and E. E. Alp, 2006
- [24] U.S. Patent granted No. 7,162,888, D. Shu, A. Joachimiak, C. Preissner, D. Nocher, Y. Han, J. Barraza, P. Lee, W. Lee, Z. Cai, S. Ginell, R. Alkire, R. Schuessler, 2007
- [25] U.S. Patent granted No. 7,331,714, D. Shu, J. Maser, B. Lai, S. Vogt, M. Holt, C. Preissner, R. Winarski, G. Stephenson, 2008
- [26] H. C. Kang et al., Phys. Rev. Lett. 96, 127401 (2006).
- [27] H. Yan et al., Apl. Phys. Lett. in print (2008)
- [28] J. Maser et al. Proc. SPIE-Int. Soc. Opt. Eng. 5539, 185 (2004).

